THE JOURNAL OF BIOLOGICAL CHEMISTRY

Vol. 269, No. 9, Issue of March 4, pp. 6716-6724, 1994
Printed in U.S.A.

Functional Properties of the Purified N-type Ca^{2+} Channel from Rabbit Brain*

(Received for publication, September 14, 1993, and in revised form, November 3, 1993)

Michel De Waard, Derrick R. Witcher, and Kevin P. Campbell‡

From the Howard Hughes Medical Institute, Department of Physiology and Biophysics, University of Iowa College of Medicine, Iowa City, Iowa 52242

N-type Ca^{2+} channels control a variety of key neuronal functions including transmitter release at synaptic terminals. The purified ω-conotoxin receptor from rabbit brain is a multisubunit complex composed of α_{1B}, $\alpha_2\delta$, β_3, and 95-kDa subunits. Immunoadsorption experiments confirm that the purified preparation does not contain α_1 subunits other than the ω-conotoxin-sensitive class B isoform. The functional properties of the purified channel have been analyzed further in lipid bilayers, and similarities to or differences from the native N-type Ca^{2+} channel have been outlined. Conserved properties include ion selectivity, open-time duration, and pharmacology (insensitivity to drugs affecting skeletal muscle L-type Ca^{2+} channels). Observed properties of the reconstituted channel which differ from the native channel include (*a*) sustained channel activity without Ca^{2+}- or voltage-induced inactivation; (*b*) examples of extremely high open-state probability; (*c*) the absence of "rundown"; and (*d*) voltage independence of the Ca^{2+} channel gating. In addition, the conductance of the purified receptor is comprised between 7 and 27 picosiemens. Our results suggest that cellular components may play critical roles in the regulation of several biophysical properties and neuronal function of the native N-type Ca^{2+} channel.

Based on their sensitivity to the neuropeptide ω-conotoxin GVIA (ω-CgTx)[1] N-type Ca^{2+} channels are involved in various neuronal processes that include membrane excitability, axonal outgrowth, neuronal migration (1), and neurotransmitter release (2). N-type Ca^{2+} channels are also directly (3) or indirectly (4) the target of pathogenic autoantibodies associated with Lambert-Eaton myasthenic syndrome. In addition to the N-type Ca^{2+} channel, biophysical and pharmacological studies have defined three more types of Ca^{2+} channels (5) termed T-, L- (6, 7), and P-type (8, 9).

Purification of the skeletal muscle DHP receptor has shown that this L-type Ca^{2+} channel is composed of four subunits: the pore-forming α_1 subunit, an $\alpha_2\delta$ subunit, a cytoplasmic and regulatory β subunit, and a γ subunit (10, 11). More recently, molecular cloning of α_1 and β subunits has demonstrated that multiple genes (12) and numerous splice variants encode these two subunits. Because α_1 subunits are often receptors for drugs or toxins that affect Ca^{2+} channel activity (13, 14), their pharmacological properties represent convenient ways to relate these subunits to native Ca^{2+} channels. Therefore, expression of cloned subunits and reconstitution of purified Ca^{2+} channels represent two useful strategies for investigating the structural and functional aspects of Ca^{2+} channels. Although numerous Ca^{2+} channel subunits have been expressed so far, the resulting channels remain under the influence of cell regulatory components and have subunit compositions that frequently do not reflect those of native channels. In contrast, the reconstitution of purified multisubunit Ca^{2+} channels is more likely to provide information about the intrinsic properties of these structures.

We have reported recently the purification of the ω-conotoxin receptor from rabbit brain and its native subunit composition (15). The receptor is composed of an α_1 subunit of 230 kDa (class B), a β_3 subunit of 57 kDa, an $\alpha_2\delta$ subunit of 150 kDa (which shares strong homology with the skeletal $\alpha_2\delta$), and a novel 95-kDa subunit. We now report the biophysical properties of the purified N-type channel upon reconstitution into bilayers. Properties of the purified ω-CgTx receptor were compared with those of the native N-type channel. Similarities include the open-time durations, the selectivity for divalent cations over monovalent cations, the selectivity among divalent cations, the insensitivity to drugs affecting L-type Ca^{2+} channels and to some extent the conductances. Differences include the open-state probability, the voltage independence of the channel gating, and the absence of inactivation. Our results strongly suggest that labile interactions between Ca^{2+} channel complexes and their cellular environment are important determinants of the biophysical properties of native Ca^{2+} channels.

EXPERIMENTAL PROCEDURES

Purification of the ω-CgTx-sensitive Ca^{2+} Channel—The ω-CgTx-sensitive Ca^{2+} channel was prepared from rabbit brain membranes as described previously (15). Five-μl aliquots of peak fractions 9, 10, and 11 were stored at −80 °C until use. The reconstitution data were obtained from more than six different preparations.

Immunoadsorption—Affinity-purified sheep polyclonal antibodies to the α_{1B} subunit of the N-type Ca^{2+} channel complex were coupled to 50 μl of protein G-Sepharose and equilibrated in 10 mM Hepes (pH 7.4), 0.5 M NaCl, 0.1 mM phenylmethylsulfonyl fluoride, and 0.75 mM benzamidine (buffer A). The immunoaffinity beads were incubated with 0.6 ml of purified N-type Ca^{2+} channels for 4 h at 4 °C. After pelleting, the supernatant (void) was decanted, and the affinity beads were washed with three aliquots of 0.5 ml of buffer A. The void from the affinity column and the three washes were pooled and concentrated in a Centricon-100. A 400-μl aliquot of the purified receptor was also concentrated in a Centricon-100. Both samples were reduced to a final volume of 300 μl. 200 μl of each sample was separated by SDS-polyacrylamide gel electrophoresis on a 3–12% gel and stained with Coomassie Blue. 50 μl of each sample was separated by SDS-polyacrylamide gel electrophoresis, transferred to nitrocellulose, and stained with affinity-purified polyclonal antibodies to the α_{1B} or 95-kDa subunits.

Bilayers—Lipid monolayers were formed at the surface of a 1.5-ml ionic solution by spreading 1–2 μl of lipids (30 mg/ml in decane) composed of phosphatidylserine and phosphatidylethanolamine in a 1:1

* The costs of publication of this article were defrayed in part by the payment of page charges. This article must therefore be hereby marked "*advertisement*" in accordance with 18 U.S.C. Section 1734 solely to indicate this fact.

‡ Investigator of Howard Hughes Medical Institute. To whom correspondence should be addressed: Howard Hughes Medical Institute, University of Iowa College of Medicine, 400 Eckstein Medical Research Bldg., Iowa City, IA 52242. Tel.: 319-335-7867; Fax: 319-335-6957.

[1] The abbreviations used are: ω-CgTx, ω-conotoxin GVIA; DHP, dihydropyridine; Hpip, holding pipette potential; pS, picosiemens.

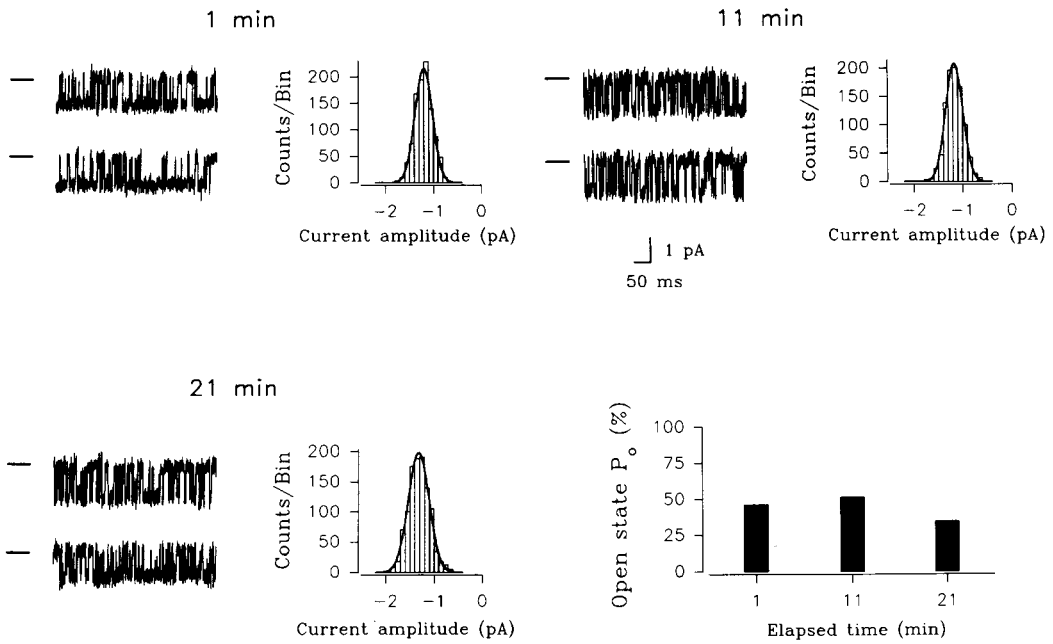

FIG. 1. **Absence of inactivation of the ω-CgTx receptor in bilayers.** Shown are trace examples, amplitude histograms, and open-state probabilities 1, 11, and 21 min after the start of channel activity. In all panels, *straight lines* denote the closed state of the channel. The mean current amplitudes are −1.2 ± 0.18 pA (n = 2,012, 1 min), −1.17 ± 0.18 pA (n = 1,890, 11 min), and −1.31 ± 0.21 pA (n = 2,126, 21 min). Amplitude histograms are fitted by $n = W \cdot \exp[-(A-\mu)^2/2\cdot\tau^2]/\sqrt{2\pi}\cdot\mu$ with W a constant equal to 646 (1 min), 611 (11 min), and 654 (21 min). n represents the counts at each amplitude, A is expressed as a current amplitude (pA), μ the mean amplitude (pA), and τ is the standard deviation (pA). Unless mentioned the bin width is always 0.1 pA/division. The *lower right* of the figure displays the open-state probability at each corresponding elapsed time. Time analyzed in each case: 12.4 s (1 min), 10.8 s (11 min), and 11.5 s (21 min). Hpip = −100 mV in symmetrical 100 mM $BaCl_2$. Recordings were filtered at 1 kHz and sampled at 5 kHz.

weight ratio. Solvent free lipid bilayers were then formed from the monolayers at the tip of heat-polished and Sylgard-coated patch electrodes (mean resistance = 7.1 ± 4.2 megohm) by the tip-dip technique (16). Only seal resistances higher than 10 gigohm were considered (mean 33.1 ± 24.7 gigohm).

Channel Incorporation and Sidedness of Ca^{2+} Channels in Lipid Bilayers—In most cases, channels were inserted directly into the monolayer by dilution into the extrapipette solution at an approximate concentration of 1 pM. Channel incorporation into the monolayer was favored by magnetic stirring of the extrapipette solution. Bilayers were then formed by the tip-dip method. In these conditions, sidedness of the channel was random. In a few other cases, channels were inserted after bilayer formation either by dilution of a sample of the purified preparation into the extrapipette solution or by preincorporation into the electrode at a final receptor concentration of 20 pM. Channel incorporation occurred either during patch formation when present in the electrode or by the use of a higher hydrostatic pressure on the side of channel addition. Further channel incorporation could easily be stopped by slightly moving the electrode in or out of the extrapipette solution. In these conditions, channel sidedness mostly occurred with the extracellular face of the channel toward the side of dilution as assessed by the polarity of ω-CgTx blockade (15).

Solutions—The extrapipette and pipette solutions contained 100 mM $BaCl_2$ (or $CaCl_2$) unless another concentration is specified in the text and 10 mM Hepes (or 5 mM if [$BaCl_2$] < 50 mM). The pH was brought to 7.4 with $Ba(OH)_2$ or Tris. All solutions were filtered twice with a 0.22-μm filter (Millipore).

Electrical Recordings—The potential across the bilayers was controlled by clamping the pipette potential (Hpip) with respect to the bath. Ground and pipette Ag/AgCl electrodes were connected to an Axopatch 200A (Axon Instruments). All recordings were leak subtracted using the leak subtraction circuit of the amplifier. By convention, positive current signals are displayed as upward deflections from the zero-current base line (except where mentioned) and reflect cationic flow from the pipette to the bath (positive Hpip). Anionic current flow in the opposite direction was excluded by measurements of the current reversal potential following a change in $BaCl_2$ concentration in the bath. After membrane formation, the gain was increased to 100 mV/pA. All recordings were performed at room temperature (20–22 °C). Single channel recordings were stored on a digital tape recorder (DTR 1202, Biologic) before filtering and analyzing.

Data Analysis—Tape data were retrieved in analogue format and postfiltered at 1–2 kHz (Frequency Devices) before digital acquisition using a LabMaster A/D interface (Axon Instruments). Data were digitized at 3–5 times the filter cutoff frequency (5–10 kHz) and stored on a PC Gateway computer. Single channel data were analyzed using PClamp 5.5.1 software (Axon Instruments). Open-state amplitudes of the channels were measured in either of two ways: (*a*) after separation of open and closed current levels using a threshold criterion set at 0.5 the predominant open channel amplitude or (*b*) by sorting all sampled current points at a gain of 0.1–0.2 pA/bin and fitting base-line and open-state levels as a sum of two Gaussian distributions. Events shorter than 0.3 ms (3 kHz filtering), 0.5 ms (2 kHz), or 1 ms (1 kHz) were not considered for open-state duration and amplitude histograms. The open-state probability (p_o) of the channel was calculated either as a ratio of the cumulative time spent in the open state to the total time of recording or was determined from the relative areas covered by closed and open states of all point amplitude histograms. A nonlinear Levenberg-Marquardt least squares curve-fitting procedure was used for fitting Gaussian (amplitude histograms) and exponential (open- and closed-time distributions) curves. Straight lines from conductances curves were least square fits to the data.

Chemicals—Verapamil was a gift from Knoll Pharmaceuticals. A 10 mM dimethyl sulfoxide stock solution of verapamil was kept at −20 °C in the dark. ω-CgTx GVIA was from Peninsula. All drugs were directly applied into the extrapipette solution. Because verapamil lacks sidedness of action (17, 18), we did not control the channel orientation. Bovine brain phosphatidylserine and phosphatidylethanolamine were purchased from Avanti Polar Lipids and stored in chloroform at −80 °C.

RESULTS

The Purified ω-CgTx Receptor Does Not Inactivate or Run Down—Fig. 1 shows that the ω-CgTx receptor forms a functional Ca^{2+} channel upon reconstitution into bilayers. Numerous controls have ensured that this activity is specifically a result of the incorporation of the purified receptor into the bilayer (15). Recordings at Hpip = −100 mV (100 mM symmetrical Ba^{2+}) 1, 11, and 21 min after patch formation show that the current amplitude of the channel remained constant within experimental error. Mean current amplitudes were −1.2 ± 0.18 pA at 1 min, −1.17 ± 0.18 pA at 11 min, and −1.31 ± 0.21 pA at 21 min, which yields an estimated conductance of 12–13 pS for

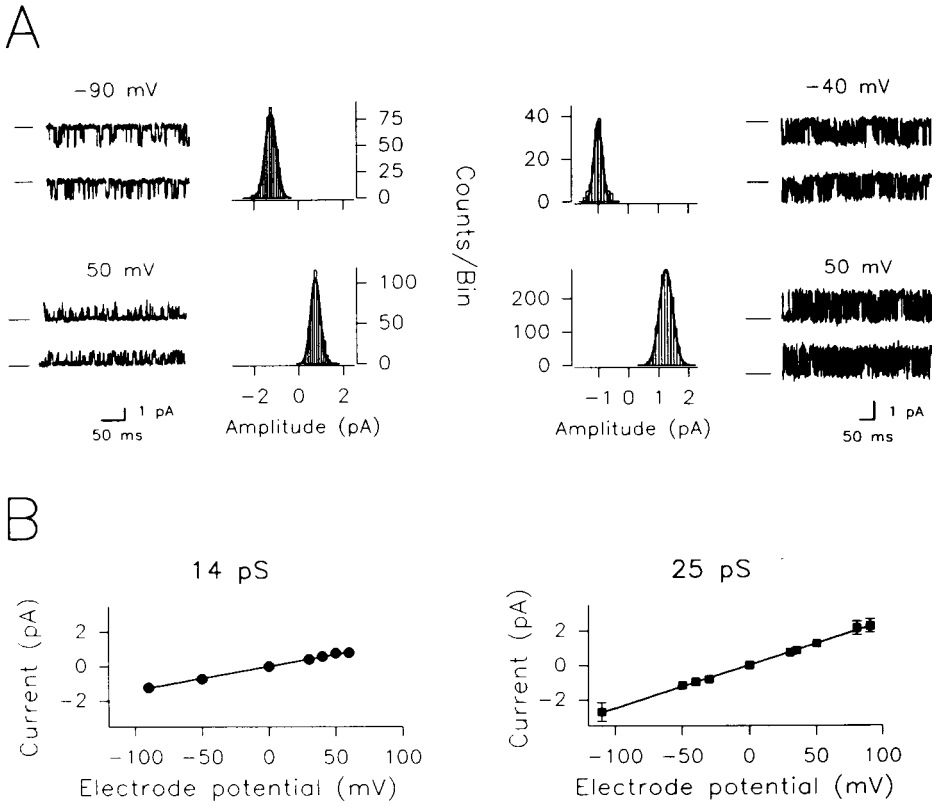

FIG. 2. **Conductances of the purified ω-CgTx receptor.** *A*, trace examples and corresponding histogram amplitudes of two main conductance forms of the ω-CgTx receptor. The *left panel* displays single channel activities and amplitude histograms of a 14-pS channel at −90 and +50 mV. Mean current amplitudes are −1.24 ± 0.24 pA (n = 520, Hpip = −90 mV) and 0.75 ± 0.21 pA (n = 584, Hpip = +50 mV). The *right panel* displays single channel activities and amplitude histograms of a 25.5-pS channel at −40 and +50 mV. Mean current amplitudes are −0.99 ± 0.14 pA (n = 154, Hpip = −40 mV) and 1.25 ± 0.22 pA (n = 1,550, Hpip = +50 mV). Filter frequencies were 1.5 kHz (14 pS) and 1 kHz (25 pS), and the sampling frequency was 5 kHz. For each conductance, the horizontal scaling of the amplitude histograms is identical for both potentials to show the shift in current amplitude. All amplitude histograms were fitted as in Fig. 1 with W = 252 (Hpip = −90 mV, 14 pS), 198 (Hpip = +50 mV, 14 pS), 93 (Hpip = −40 mV, 25 pS) and 899 (Hpip = +50 mV, 25 pS). *B*, corresponding Hpip-current amplitude relation for the 14- (*circles*, *left panel*) and 25-pS (*squares*, *right panel*) channels. Both channels reversed at 0 mV as expected in symmetrical 100 mM $BaCl_2$. Each experimental point represents the mean current amplitude (±S.D.) of individual amplitude histograms based on 440–580 (14 pS) and 131–1,599 counts (25 pS). Conductances were obtained by fitting the data with first order regression lines. Undetected error bars are within symbol limits.

this channel. The corresponding open-state probabilities remained high throughout the experiment and were 46.2, 51.5, and 34.7% at 1, 11, and 21 min, respectively. Since channel activity remained sustained over long periods of time, we concluded that the purified channel does not run down or inactivate. Similar results were obtained at various Hpip and channel conductances (not shown).

The Purified ω-CgTx Receptor Displays a Variety of Conductances upon Reconstitution—Reconstituted channels had conductances ranging between 7 and 27 pS in symmetrical 100 mM $BaCl_2$ (n = 26). The mean conductance was 18 ± 5 pS. Fig. 2*A* illustrates recordings of a 14-pS (*left panel*) and a 25-pS channel (*right panel*). In both cases, channel activity was sustained at each Hpip, and unitary current amplitudes followed single Gaussian distributions. Mean current amplitudes for these channels were −1.24 ± 0.24 pA at Hpip = −90 mV and 0.75 ± 0.21 pA at Hpip = +50 mV (14-pS channel), and −0.99 ± 0.14 pA at Hpip = −40 mV and 1.25 ± 0.22 pA at Hpip = +50 mV (25-pS channel). Current-voltage plots for the 14- and 25-pS channels show linear relationships over a wide range of potentials (Fig. 2*B*). In some experiments, the recordings displayed higher and more complex conductance behaviors suggesting multiple channel incorporations. These cases were not analyzed further.

Purified N-type Ca^{2+} Channels Have Two Gating Patterns—Recordings could be divided into two gating patterns. Fig. 3 illustrates this segregation for two recordings of similar conductances around 24–25 pS. The first gating pattern is characterized by a single exponential distribution with an open-time constant of τ_o = 2.1 ms and a low open-state probability of p_o = 5.1% at Hpip = −110 mV (Fig. 3, *upper panel*). Channels with single open-time distributions had an average p_o of 12.5% with individual values ranging from 2.7 to 23.7% (n = 7/21). The 14-pS channel of Fig. 2*A* is a representative recording of a low-p_o pattern. In contrast, the second gating pattern is characterized by a double exponential distribution with open-time constants of τ_{o1} = 1.6 ms and τ_{o2} = 7.8 ms and an open-state probability of p_o = 82.3% at Hpip = 50 mV. Channels with double open-time distributions were characterized by much higher open-state probabilities with an average p_o of 66.1% (n = 14/21) and individual values comprised between 33 and 96.7%. The 25-pS channel of Fig. 2*A* and the 12–13-pS channel of Fig. 1 are representative recordings of the high p_o gating. Fig. 1 demonstrates that no conversions between p_o states (either randomly or induced by voltage modifications) could be detected within single recordings. This suggests that each of these modes is driven by stable states of the channels.

Selectivity—Recordings in asymmetrical ionic conditions (100 mM $BaCl_2$ pipette and 100 mM $CaCl_2$ extrapipette) show that Ba^{2+} was almost three times more permeant than Ca^{2+} through ω-CgTx-sensitive Ca^{2+} channels (Fig. 4, *A–C*). This result is consistent with the reported selectivity of the native ω-CgTx receptor (7) or of the cardiac DHP receptor in bilayers (19). In agreement with conserved selectivities of the channel is the finding that the channels were not permeable to Na^+ (n = 8)

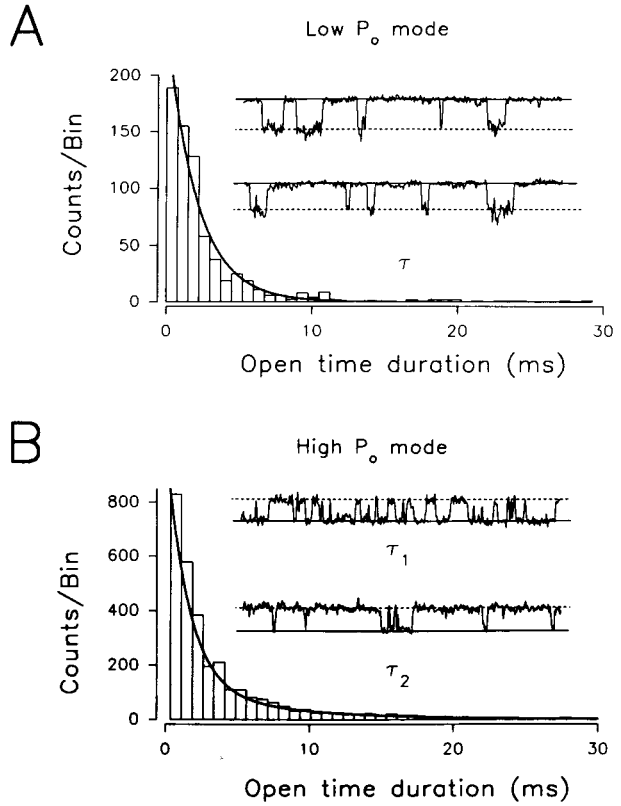

FIG. 3. **Gating pattern of the N-type Ca^{2+} channel.** Open-state duration histograms for low and high opening probabilities of two 24–25-pS channels. Time constants (τ) and corresponding opening probabilities (p_o) are τ = 2.1 ms and p_o = 5.1% (over 37 s) for low p_o, and τ_1 = 1.6 ms (62.9% of openings), τ_2 = 7.8 ms (37.1% of openings) and p_o = 82.3% (over 16.8 s) for high p_o. The bin width is 0.75 ms/division. Open-time distributions were fitted by $n = W_n/\tau_n \cdot \exp(T/\tau_n)$ with W_n constant (W = 514, low p_o; W_1 = 1,463 and W_2 = 864, high p_o). n represents the counts at each open-state duration with totals of 699 (low p_o) and 1,599 (high p_o). The *insets* are trace examples of each case. Recordings were filtered at 3 kHz and sampled at 10 kHz for display and analysis. Trace lengths are 50 ms. *Straight* and *dashed lines* represent the closed and open states of the channels, respectively. Hpip was −110 mV (low p_o) and 50 mV (high p_o).

or K^+ (n = 9), even at concentrations 20 times greater than used normally and over periods of observation (10–20 min) which should ensure channel presence (Fig. 4*D*). These results suggest that the purified channel has conserved the structural requirements for a selective permeability.

Symmetrical Ba^{2+} Concentration-Conductance Relationship—We have plotted the mean conductance value of the N-type Ca^{2+} channel as a function of the symmetrical Ba^{2+} concentration for recordings of the N-type Ca^{2+} channel (Fig. 5). We show that single channel recordings can still be obtained with significant decreases in Ba^{2+} concentration. The fit of the data yields a maximum mean conductance of 19.8 pS and a Ba^{2+} concentration responsible for a half-maximal conductance of 19.2 mM. Conductance was almost maximal at 60 mM Ba^{2+}, whereas at 10 mM Ba^{2+} the mean conductance value of the channel is 6.1 ± 1.7 (n = 4).

Gating of the Purified ω-CgTx Receptor Lacks Voltage Dependence—We consistently failed to observe voltage-induced changes in the gating of the purified ω-CgTx receptor. Fig. 6, *A* and *B*, illustrates the example of a 14-pS channel in a low p_o state. A Hpip modification from −50 to +50 mV did not significantly affect the open-time constant of this channel (Fig. 6*A*, *upper panel*). As in the case of Fig. 3, the channel had fast openings with mean open-time durations of τ_o = 1.87 ms at Hpip = −50 mV and τ_o = 1.08 ms at +50 mV. The corresponding closed-time distributions were best described by two-exponential fits (Fig. 6*A*, *lower panel*). Again, voltage modification had no significant effect on closed-time constants with τ_{c1} = 4.03 ms and τ_{c2} = 12.04 ms at Hpip = −50 mV compared with τ_{c1} = 2.9 ms and τ_{c2} = 8.6 ms at Hpip = +50 mV. The voltage dependence of open- and closed-time constants has been represented at various Hpip values in Fig. 6*B*. The corresponding plot of open-state probability of the channel at various Hpip values confirms the absence of voltage dependence of the channel (Fig. 6*C*).

Opposite orientation of two or more channels is unlikely to account for these observations because switching the Hpip polarity of all of our recordings did not modify the number of functional channels, their conductances, or their gating patterns. We ruled out orientation as a basis for the observed voltage independence by using ω-CgTx as a tool to control the polarity of functional channels in bilayers. Functional block of channel activity by ω-CgTx is experimentally complex because binding of the toxin to its receptor is inhibited by high divalent cation concentrations necessary for channel recordings (20). We have shown previously that single channel activity was blocked by ω-CgTx at 10 mM Ba^{2+} (15). In these conditions, however, the addition of 0.5 μM ω-CgTx to the electrode side does not prevent the occurrence of single channel activity at potentials of opposite polarities (Fig. 6*D*, *left traces*). The voltage independence of this high p_o channel is illustrated by the maintenance of invariant open-state probabilities of 97.7% at −140 mV *versus* 99% at +160 mV (Fig. 6*D*, *right panel*).

Only α_1 Class B Isoforms Are Present in the Purified Preparation—Previous experiments have shown that DHP-sensitive α_1 subunits were absent from the purified preparation (15). We have further assessed the subunit association of the ω-CgTx receptor by immunoaffinity adsorption. Immunoaffinity beads were prepared with affinity-purified polyclonal antibodies against the predicted loop between the second and third transmembrane repeats of the α_1 class B (21) and were incubated with the purified receptor complex. SDS-polyacrylamide gel electrophoresis analysis of the void demonstrated that the α_{1B} immunoaffinity beads selectively adsorbed virtually all of the receptor complex. Western blot analysis of the same void also verified that α_{1B} and 95-kDa subunits were selectively adsorbed to the immunoaffinity beads (Fig. 7*A*) along with $\alpha_2\delta$ and β_3 (not shown). Immunoblots of immunoaffinity beads separated on gels indicated that all of the subunits of the receptor complex were retained by the beads and not proteolyzed during immunoprecipitation (not shown).

We have reported previously the absence of effects of DHP compounds on the purified N-type Ca^{2+} channel (15). We investigated further the effects of verapamil, a phenylalkylamine compound, since there is a report of Ca^{2+} currents sensitive to DHPs but not phenylalkylamines (22), and the cloned human α_1 class D subunit is sensitive to both DHP and ω-CgTx (23). The application of 1 μM verapamil on a high p_o state channel activity did not modify the channel amplitude or its open-state probability (Fig. 7*B*, n = 3). Current amplitudes at Hpip = +100 mV remained constant with mean values of 1.97 ± 0.36 pA (control) compared with 1.96 ± 0.38 pA (verapamil), yielding an estimated conductance close to 20 pS. Open-state probabilities derived from all point amplitude histograms were 96.7% (control) compared with 95% (verapamil). Longer exposures of the channel to the drug had no significant effects either.

DISCUSSION

Published results show that two Ca^{2+} channels have been purified, the DHP receptor from skeletal muscle (10, 11) and recently the N-type Ca^{2+} channel (15, 24). These reports show that Ca^{2+} channels are multisubunit complexes composed of an α_1 subunit, a conserved $\alpha_2\delta$ subunit, a β subunit, and an addi-

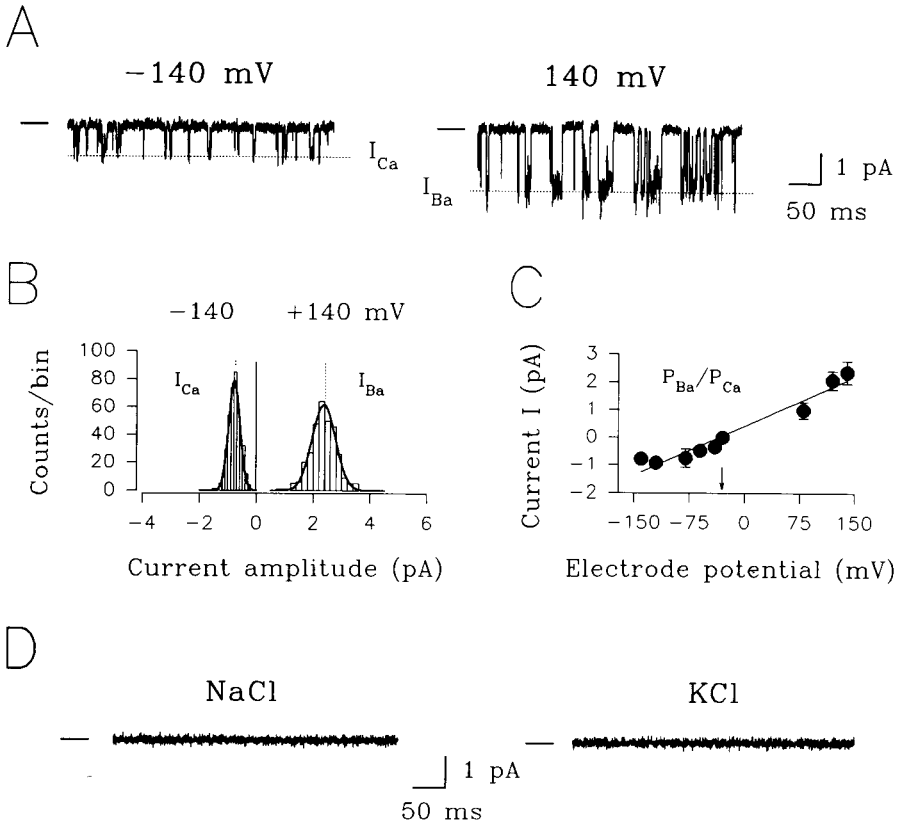

FIG. 4. **Selectivity of the ω-CgTx receptor.** *A*, trace examples of a recording in asymmetrical ionic conditions. The electrode and extrapipette medium contained 100 mM $BaCl_2$ and 100 mM $CaCl_2$, respectively. At a negative driving force (Hpip = −140 mV) Ca^{2+} permeability is favored, whereas at a positive driving force (Hpip = +140 mV) Ba^{2+} permeability is favored. Note the larger unitary amplitude recorded when Ba^{2+} is the main permeant cation. The polarity of recording at Hpip = +140 mV was inverted to facilitate current amplitude comparisons. *Dashed lines* represent the open state of the channel. Recordings were filtered at 2 kHz and sampled at a 10-kHz frequency. *B*, corresponding amplitude histograms at Hpip = −140 and +140 mV. Mean current amplitude are I_{Ca} = −0.776 ± 0.199 pA (n = 399, Hpip = −140 mV) and I_{Ba} = 2.37 ± 0.41 pA (n = 314, Hpip = +140 mV). Fit of amplitude histograms gave W = 139 (Hpip = −140 mV) and 358 (Hpip = +140 mV). The bin widths are 0.1 (Hpip = −140 mV) and 0.2 (Hpip = +140 mV) pA/division. *Straight* and *dashed lines* show the zero and mean current levels, respectively. *C*, corresponding Hpip-current relation. Each point is the mean amplitude (±S.D.) of between 82 and 507 openings. The conductance is 12.7 pS in these conditions. The *arrow* shows the measured reversal potential (E_{rev} = −30 mV). The Ba^{2+}/Ca^{2+} permeability ratio is P_{Ba}/P_{Ca} = 2.8 assuming a Cl^- permeability of zero. This value was calculated based on the Goldman-Hodgkin-Katz equation for two permeant cations with $E_{rev} = RT/zF \cdot \ln(P_{Ca} \cdot [Ca]/P_{Ba} \cdot [Ba])$ where R, T, and F have their usual meanings, and the cation valence is z = 2. *D*, the absence of Na^+ or K^+ permeability. Solutions on both sides of the bilayer were 150 mM NaCl or KCl, 5 mM $CaCl_2$, and 10 mM Hepes (pH = 7.4). $CaCl_2$ was present at low concentrations to ensure bilayer stability. The receptor concentration was 20 pM, a 20-fold increase over the concentration used normally. Recordings were filtered at 2 kHz and sampled at 5 kHz.

tional more variable subunit. Coexpression experiments of various subunits have further strengthened the presumption that Ca^{2+} channels could have conserved subunit compositions (25–27). Although the role of the $\alpha_2\delta$ subunit remains largely unclear, all β subunits seem able to enhance the expression and function of the α_1 subunit (26, 28, 29) with the notable exception of the α_{1E} (30). Surprisingly, this holds true for various β subunit isoforms encoded by multiple genes when expressed with a single α_1 isoform (29, 31, 32) although the purification data suggest more specificity in the interactions between these two subunits (15). Whether such discrepancies could be explained by differences in the level of expression of β subunits in various tissues as suggested by Hulin *et al.* (31) remains largely to be investigated. Because Ca^{2+} channels seem to have conserved structural features, it is not surprising that the purified ω-CgTx receptor shares many properties with the purified DHP receptor from skeletal muscle.

Our data show that Ca^{2+} channel activity in bilayers is sustained for periods that largely exceed those reported for native Ca^{2+} channels. It is well known that native voltage-dependent Ca^{2+} channels undergo a rapid process of decreased activity termed "run-down" (23, 30). This process takes place within seconds (upon patch excision) or minutes (upon cell dialysis in the whole-cell recording mode of patch-clamp) and was initially

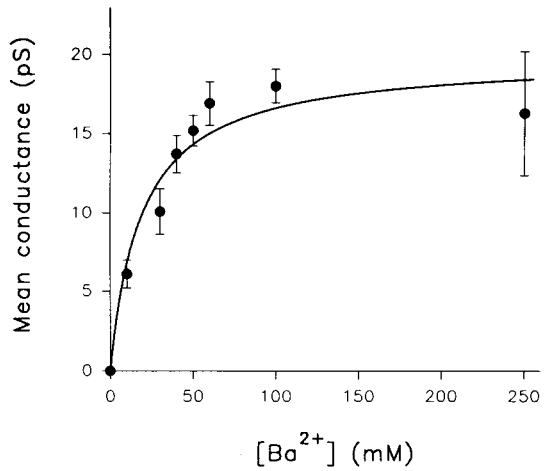

FIG. 5. **Relation between Ba^{2+} concentration and conductance.** Shown are the average conductance values *versus* symmetrical $BaCl_2$ concentration. Each point is the mean of between n = 3 and 26 experiments (±S.E., total experiments n = 61). The data are fitted with a hyperbolic function $g_{Ba} = g_{max} \cdot [Ba]/([Ba]_{1/2} + [Ba])$ where g_{Ba} is the mean conductance, g_{max} the maximum conductance (g_{max} = 19.8 pS), [Ba] the symmetrical $BaCl_2$ concentration, and $[Ba]_{1/2}$ the Ba^{2+} concentration responsible for half the maximal conductance ($[Ba]_{1/2}$ = 19.2 mM).

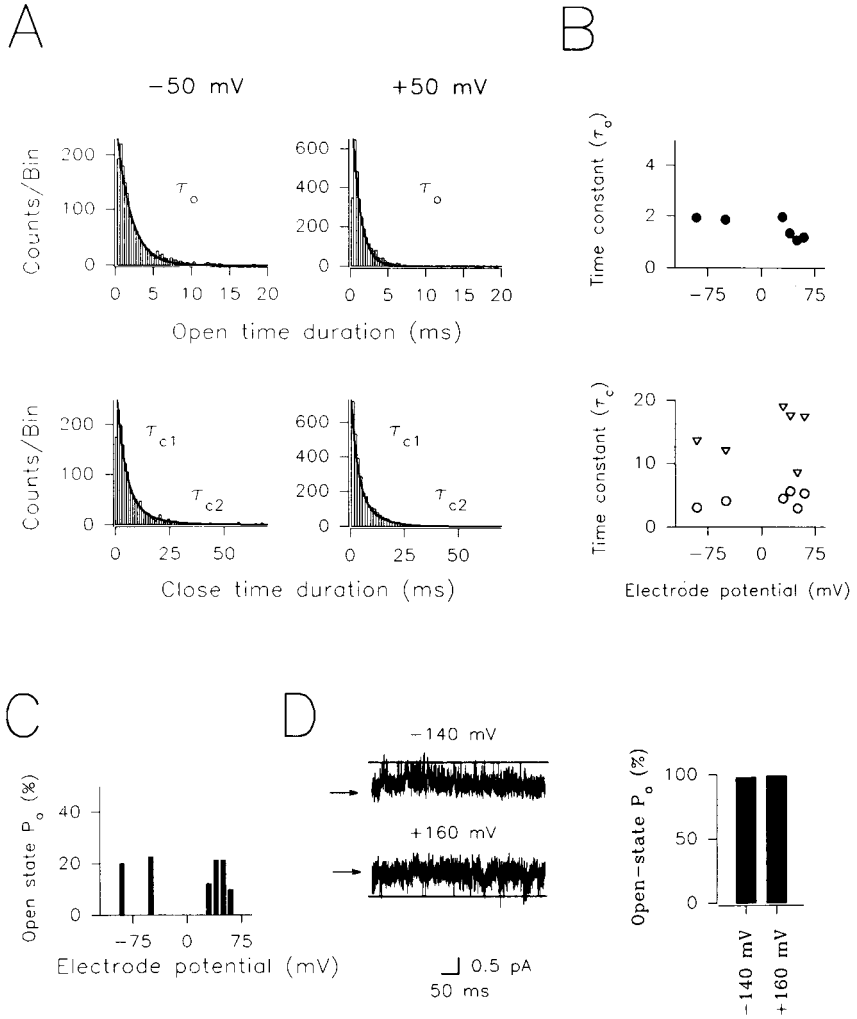

FIG. 6. **Lack of voltage dependence of the N-type Ca^{2+} channel gating.** *A*, open- and closed-time distributions of a low p_o state channel at two opposite electrode potentials. Open-time distributions (*upper panel*) were best described with single exponentials. Open-time constants (τ_o) are 1.87 ms (−50 mV) and 1.08 ms (+50 mV). Corresponding closed-time distributions (*lower panel*) were best described by the sum of two exponentials. Closed-time constants (τ_c) are τ_{c1} = 4.03 ms and τ_{c2} = 12.04 ms (−50 mV), and τ_{c1} = 2.9 ms and τ_{c2} = 8.6 ms (+50 mV). Distributions were fitted as usual. *W* values were 513 (−50 mV) and 1,053 (+50 mV) for open-time distributions, and 1,037–604 (W_1-W_2, −50 mV) and 1811–2062 (W_1-W_2, +50 mV) for closed-time distributions. *n* represents the number of counts for each bin with totals of 1,606 (−50 mV) and 3,056 (+50 mV). Recordings were filtered at 2.5 kHz and sampled at 10 kHz prior to analysis. Events faster than 300 μs were ignored. The conductance of the channel was 14 pS in symmetrical 100 mM $BaCl_2$. *B*, open- and closed-time constants *versus* Hpip. Same recording as in *A*. *Filled circles* (τ_o in ms) represent time constants of single exponential fits to open-time distributions at six different potentials. *Open circles* (τ_{c1} in ms) and *open triangles* (τ_{c2} in ms) are time constants of two-exponential fits to the corresponding closed-time distributions at the same potentials. Distributions contained from 1,412 to 3,060 counts totally. Open-state probability was computed from 21.2–33.2-second recordings. *C*, corresponding open-state probability *versus* Hpip. *D*, high p_o channel activity in symmetrical 10 mM $BaCl_2$. 0.5 μM ω-CgTx was added on the electrode side to block eventual Ca^{2+} channels of opposite polarity of insertion. Open-state probabilities were compared at two opposite potentials for recordings of 27 (−140 mV) and 29 s (+160 mV). *Arrows* show the open state. Traces were 512 ms in length, filtered at 2 kHz, and sampled at 10 kHz. The conductance of the channel is 6.3 ± 1.3 pS.

defined as a multifactorial process that involves dephosphorylation and/or proteolysis under native conditions (34). Because the ω-CgTx receptor does not need to be *in vitro* phosphorylated to display channel activity, we conclude that dephosphorylation and proteolysis are not *per se* primary causes for run-down. However, we cannot rule out that some degree of endogenous phosphorylation of the purified receptor ensures channel activity. Variable levels of endogenous phosphorylation could further explain variable conductances and multiple open-state probabilities of the channels upon reconstitution.

The purified ω-CgTx receptor displays more than a single conductance upon reconstitution into bilayers. However, such a conductance variability is not limited to the purified channel since recordings of the N-type Ca^{2+} channel reveal conductances of 11 pS in superior cervical ganglia neurons (2), 13 pS in chick dorsal root ganglion neurons (7) and 19 and 20.6 pS in PC12 cells and superior cervical ganglia neurons (35). This suggests that, contrary to general belief, conductances cannot be used as a reliable criterion for the identification of the channel type. A similar conclusion has recently been reached on a study of the P-type Ca^{2+} channel (9). We discuss several possibilities that might explain the variability in conductances of the purified ω-CgTx receptor.

Our data show that the purified ω-CgTx receptor from rabbit brain contains only α_1 class B isoforms. The absence of non-class B α_1 isoforms is further evidenced by an absence of sensitivity of the purified channel to agonists and antagonist of L-type Ca^{2+} channels (15). Westenbroek *et al.* (36) and Dubel *et al.* (21) have suggested the existence of more than a single ω-CgTx-sensitive α_{1B} isoform in rabbit brain. Whether the conductance variability that we report arises to some extent from ω-CgTx-sensitive α_{1B} isoforms is not known.

It is likely that subpopulations of Ca^{2+} channels exist in the purified preparation with different regulatory states (*i.e.* phosphorylated *versus* nonphosphorylated). Such a presumption is strengthened by the presence of two main gating patterns of

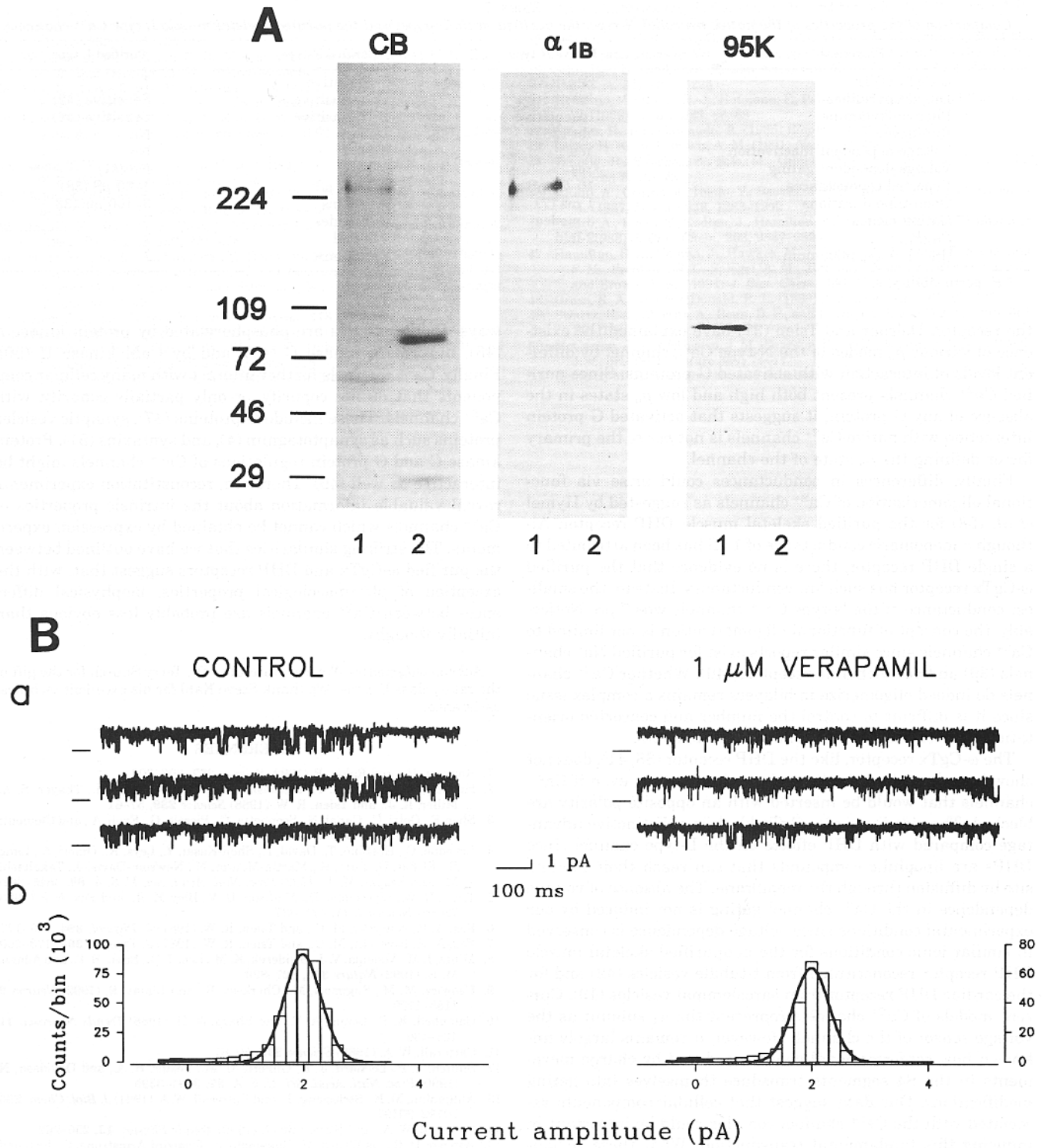

FIG. 7. **Immunoadsorption and verapamil sensitivity of the N-type Ca^{2+} channel.** *A*, immunoadsorption. Peak fractions 8 and 9 of the purified N-type Ca^{2+} channel from sucrose density gradients were as described (15) before (*lane 1*) and after (*lane 2*, void) the α_{1B} affinity column. Samples were separated by SDS-polyacrylamide gel electrophoresis and stained with Coomassie Blue (*CB*) or transferred to nitrocellulose and stained with affinity-purified sheep polyclonal antibodies to the α_{1B} subunit (α_{1B}) or the 95-kDa subunit (*95K*) as described previously (15). Molecular mass standards ($\times 10^3$) are indicated on the *left*. Bands around 29 and 90 kDa within *lane 2* of the Coomassie Blue staining represent heavy and light chains of the polyclonal antibodies from the affinity column. *B*, effect of verapamil on channel activity. *a*, trace examples of a single Ca^{2+} channel before and after application of 1 μM verapamil. *Left panel*, control recordings; *right panel*, same recording after 1 μM verapamil application in the extrapipette medium. Trace length: 1024 ms in each case; 2-kHz filter frequency and 10-kHz sampling frequency. *b*, all-points amplitude histograms before (*left*) and after (*right*) 1 μM verapamil application. Same patch as in *A*. *Black bars* represent the closed state of the channel. Mean current amplitudes and open-state probabilities are, respectively, 1.97 ± 0.36 pA and 96.7% (control) and 1.96 ± 0.38 pA and 95% (verapamil). Intermediate events between closed and open states of the channel are because of incomplete closures of the channel. Fitting of the data yielded $W = 460{,}723$ (control) and 320,527 (verapamil). 26 and 25.8 s were analyzed in control and verapamil conditions, respectively. The bin width is 0.2 pA/division.

TABLE I

Comparison of the properties of the native neuronal N-type, the purified brain N-type, and the purified skeletal muscle L-type Ca^{2+} channels

Properties	Native N-type	Purified N-type	Purified L-type
ω-CgTx GVIA	Sensitive	Sensitive	?
Dihydropyridines	Insensitive	Insensitive	Sensitive (42)
Phenylalkylamine	Insensitive	Insensitive	Sensitive (42)
Run-down	Yes (35)	No	No
Voltage-dependent inactivation	Yes	No	No
Voltage-dependent gating	Yes	No	No (41)
Reported conductances	10–22 pS	7–27 pS	1–80 pS (38)
Open-time durations	1 ms (7)	1–7 ms	3–100 ms (33)
Gating modes	3 modes	2 modes	?
P_{Ba}/P_{Ca}[a]	2-fold	3-fold	?
$[Ba^{2+}] \rightarrow g_{Ba}$ maximum	?	≈60 mM	?

[a] *P*, permeability.

the receptor. Delcour and Tsien (37) have explained the existence of various p_o modes of the N-type Ca^{2+} channel by different levels of interaction with activated G proteins. Since purified Ca^{2+} channels present both high and low p_o states in the absence of any G protein, it suggests that activated G protein interaction with native Ca^{2+} channels is not *per se* the primary factor defining the p_o state of the channel.

Finally, differences in conductances could arise via functional oligomerization of Ca^{2+} channels as suggested by Hymel *et al.* (38) for the purified skeletal muscle DHP receptor. Although a monomeric conductance of 1 pS has been attributed to a single DHP receptor, there is no evidence that the purified ω-CgTx receptor has such low conductances. Instead, the smallest conductance of the N-type Ca^{2+} channels was 7 pS. Noticeably, the concept of functional oligomerization is not limited to Ca^{2+} channels since similar reports exist for purified Na^+ channels (39) and acetylcholine receptors (40). Whether Ca^{2+} channels do indeed oligomerize in bilayers remains a complex issue since it is difficult to control the number and concerted orientation of reconstituted Ca^{2+} channels in bilayers.

The ω-CgTx receptor, like the DHP receptor (38, 41), does not show any clear sign of voltage-dependent gating, even if Ca^{2+} channels that would be inserted with an opposite polarity are blocked. The sidedness of ω-CgTx block is a distinctive advantage compared with DHP effects on the L-type channel since DHPs are lipophilic compounds that can reach their binding site by diffusion through the membrane. The absence of voltage dependence in the Ca^{2+} channel gating is not induced by our experimental conditions since voltage dependence is conserved in similar ionic conditions for the nonpurified skeletal muscle DHP receptor reconstituted from t-tubule vesicles (42) and for the cardiac DHP receptor from sarcolemmal vesicles (19). Current models of Ca^{2+} channels represent the α_1 subunit as the voltage sensor of the channel. However, it remains largely unknown how conformational changes induced by charge movements in the S4 segments transduce themselves into gating modifications. Our data suggest that cellular components associated with the Ca^{2+} channel complex could be important in inducing this fundamental transduction. What these regulatory components might be remains largely speculative at this stage. However, it is interesting to notice that activated G proteins are able to modify the voltage dependence of native Ca^{2+} channels (43, 44) and regulate nonpurified DHP-sensitive Ca^{2+} channels in bilayers (45–47). Whether G protein interactions with Ca^{2+} channels could explain the whole voltage dependence of native Ca^{2+} channels remain to be seen.

Some noticeable differences exist between the purified receptor and its native counterpart. Interestingly, similar discrepancies have been observed between native L-type Ca^{2+} channels and purified DHP receptor (Table I). Of primary importance in the interpretation of these discrepancies is the fact that native Ca^{2+} channels may be regulated intracellularly in a number of ways. Ca^{2+} channels are phosphorylated by protein kinase A (48), by protein kinase C (49), and by CaM kinase II (50). Finally, Ca^{2+} channels further interact with many cellular components that do not copurify, or only partially copurify, with Ca^{2+} channels. These include G proteins (47), synaptic vesicles proteins such as synaptotagmin (4), and syntaxins (51). Protein kinase C and G protein regulations of Ca^{2+} channels might be interactive as well (49). Therefore, reconstitution experiments reveal valuable information about the intrinsic properties of Ca^{2+} channels which cannot be obtained by expression experiments. The striking similarities that we have outlined between the purified ω-CgTx and DHP receptors suggest that, with the exception of pharmacological properties, biophysical differences between Ca^{2+} channels are probably less obvious than initially thought.

Acknowledgments—We are grateful to Dr. Terry Snutch for the gift of the rat α_1 class B clone. We thank Steve Kahl for his excellent technical assistance.

REFERENCES

1. Komuro, H., and Rakic, P. (1992) *Science* **257,** 806–809
2. Hirning, L. D., Fox, A. P., McCleskey, E. W., Olivera, B. M., Thayer, S. A., Miller, R. J., and Tsien, R. W. (1988) *Science* **239,** 57–61
3. Sher, E., Gotti, C., Canal, N., Scoppetta, C., Piccolo, G., Evoli, A., and Clementi, F. (1989) *Lancet* **2,** 640–643
4. Leveque, C., Hoshino, T., David, P., Shoji-Kasai, Y., Leys, K., Omori, A., Lang, B., El Far, O., Sato, K., Martin-Moutot, N., Newsom-Davis, J., Takahashi, M., and Seagar, M. J. (1992) *Proc. Natl. Acad. Sci. U. S. A.* **89,** 3625–3629
5. Tsien, R. W., Lipscombe, D., Madison, D. V., Bley, K. R., and Fox, A. P. (1988) *Trends Neurosci.* **11,** 431–437
6. Fox, A. P., Nowycky, M. C., and Tsien, R. W. (1987) *J. Physiol.* **394,** 149–172
7. Fox, A. P., Nowycky, M. C., and Tsien, R. W. (1987) *J. Physiol.* **394,** 173–200
8. Mintz, I. M., Venema, V. J., Swiderek, K. M., Lee, T. D., Bean, B. P., and Adams, M. E. (1992) *Nature* **355,** 827–829
9. Usowicz, M. M., Sugimori, M., Cherksey, B., and Llinas, R. (1992) *Neuron* **9,** 1185–1199
10. Campbell, K. P., Leung, A. T., and Sharp, A. H. (1988) *Trends Neurosci.* **11,** 425–430
11. Catterall, W. A. (1988) *Science* **242,** 50–61
12. Snutch, T. P., Leonard, J. P., Gilbert, M. M., Lester, H. A., and Davidson, N. (1990) *Proc. Natl. Acad. Sci. U. S. A.* **87,** 3391–3395
13. Ahlijanian, M. K., Striessnig, J., and Catterall, W. A. (1991) *J. Biol. Chem.* **266,** 20192–20197
14. Catterall, W. A., and Striessnig, J. (1992) *Trends Physiol.* **13,** 256–262
15. Witcher, D. R., De Waard, M., Sakamoto, J., Franzini-Armstrong, C., Pragnell, M., Kahl, S. D., and Campbell, K. P. (1993) *Science* **261,** 486–489
16. Hanke, W., Methfessel, C., Wilmsen, U., and Boheim, G. (1984) *Bioelectrochem. Bioenerget.* **12,** 329–339
17. Coronado, R., and Affolter, H. (1986) in *Ion Channel Reconstitution* (Miller, C., ed) pp. 483–505, Plenum Publishing Co., New York
18. Valdivia, H. H., and Coronado, R. (1990) *J. Gen. Physiol.* **95,** 1–27
19. Rosenberg, R. L., Hess, P., and Tsien, R. W. (1988) *J. Gen. Physiol.* **92,** 27–54
20. Sakamoto, J., and Campbell, K. P. (1991) *J. Biol. Chem.* **266,** 18914–18919
21. Dubel, S. J., Starr, T. V. B., Hell, J., Ahlijanian, M. K., Enyeart, J. J., Catterall, W. A., and Snutch, T. P. (1992) *Proc. Natl. Acad. Sci. U. S. A.* **89,** 5058–5062
22. De Waard, M., Feltz, A., and Bossu, J. L. (1991) *Eur. J. Neurosci.* **3,** 771–777
23. Williams, M. E., Brust, P. F., Feldman, D. H., Patthi, S., Simerson, S., Maroufi, A., McCue, A. F., Velicelebi, G., Ellis, S. B., and Harpold, M. E. (1992) *Science* **257,** 389–395
24. McEnery, M. W., Snowman, A. M., Sharp, A. H., Adams, M. E., and Snyder, S. H. (1991) *Proc. Natl. Acad. Sci. U. S. A.* **88,** 11095–11099
25. Perez-Reyes, E., Kim, H. S., Lacerda, A. E., Horne, W., Wei, X., Rampe, D., Campbell, K. P., Brown, A. M., and Birnbaumer, L. (1989) *Nature* **340,**

233–236
26. Singer, D., Biel, M., Lotan, I., Flockerzi, V., Hofmann, F., and Dascal, N. (1991) *Science* **253,** 1553–1557
27. Williams, M. E., Feldman, D. H., McCue, A. F., Brenner, R., Velicelebi, G., Ellis, S. B., and Harpold, M. M. (1992) *Neuron* **8,** 71–84
28. Wei, X., Perez-Reyes, E., Lacerda, A. E., Schuster, G., Brown, A. M., and Birnbaumer, L. (1991) *J. Biol. Chem.* **266,** 21943–21947
29. Perez-Reyes, E., Castellano, A., Kim, H. S., Bertrand, P., Baggstrom, E., Lacerda, A. E., Wei, X., and Birnbaumer, L. (1992) *J. Biol. Chem.* **267,** 1792–1797
30. Soong, T. W., Stea, A., Hodson, C. D., Dubel, S. J., Vincent, S. R., and Snutch, T. P. (1993) *Science* **260,** 1133–1136
31. Hulin, R., Singer-Lahat, D., Freichel, M., Biel, M., Dascal, N., Hofmann, F., and Flockerzi, V. (1992) *EMBO J.* **11,** 885–890
32. Itagaki, K., Koch, W. J., Bodi, I., Klockner, U., Slish, D. F., and Schwartz, A. (1992) *FEBS Lett.* **297,** 221–225
33. Pelzer, D., Cavalie, A., Flockerzi, V., Hofmann, F., and Trautwein, W. (1988) in *The Calcium Channel: Structure, Function, and Implication* (Morad, M., Nayler, W. G., Kazda, S., and Schramm, M., eds) pp. 217–230, Springer Verlag, New York
34. Chad, J. E., and Eckert, R. (1986) *J. Physiol.* **378,** 31–51
35. Plummer, M. R., Logothetis, D. E., and Hess, P. (1989) *Neuron* **2,** 1453–1463
36. Westenbroek, R. E., Hell, J. W., Warner, C., Dubel, S. J., Snutch, T. P., and Catterall, W. A. (1992) *Neuron* **9,** 1099–1115
37. Delcour, A. H., and Tsien, R. W. (1993) *Science* **259,** 980–984
38. Hymel, L., Striessnig, J., Glossmann, H., and Schindler, H. (1988) *Proc. Natl. Acad. Sci. U. S. A.* **85,** 4290–4294
39. Boheim, G., Hanke, W., Barhanin, J., Pauron, D., and Lazdunski, M. (1985) *Molecular Basis of Nerve Activity*, pp. 131–144, Walter de Gruyter, Berlin
40. Schindler, H., Spillecke, F., and Neumann, E. (1984) *Proc. Natl. Acad. Sci. U. S. A.* **81,** 6222–6226
41. Flockerzi, V., Oeken, H.-J., Hofmann, F., Pelzer, D., Cavalie, A., and Trautwein, W. (1986) *Nature* **323,** 66–68
42. Affolter, H., and Coronado, R. (1985) *Biophys. J.* **48,** 341–347
43. Lopez, H. S., and Brown, A. M. (1991) *Neuron* **7,** 1061–1068
44. Taussig, R., Sanchez, S., Rifo, M., Gilman, A. G., and Belardetti, F. (1992) *Neuron* **8,** 799–809
45. Yatani, A., Codina, J., Imoto, Y., Reeves, J. P., Birnbaumer, L., and Brown, A. M. (1987) *Science* **238,** 1288–1292
46. Yatani, A., Imoto, Y., Codina, J., Hamilton, S., Brown, A. M., and Birnbaumer, L. (1988) *J. Biol. Chem.* **263,** 9887–9895
47. Hamilton, S. L., Codina, J., Hawkes, M. J., Yatani, A., Sawada, T., Strickland, F. M., Froehner, S. C, Spiegel, A. M., Toro, L., Stefani, E., Birnbaumer, L., and Brown, A. M. (1991) *J. Biol. Chem.* **266,** 19528–19535
48. Gross, R. A., and MacDonald, R. L. (1989) *J. Neurophysiol.* **61,** 97–105
49. Swartz, K. J., Merritt, A., Bean, B. P., and Lovinger, D. M. (1993) *Nature* **361,** 165–168
50. McCarron, J. G., McGeown, J. M., Reardon, S., Ikebe, M., Fay, F. S., and Walsh, J. V., Jr. (1992) *Nature* **357,** 74–77
51. Bennett, M. K., Calakos, N., and Scheller, R. H. (1992) *Science* **257,** 255–259